SPE-180064-MS

Transport Properties of Functionalised Silica Nanoparticles in Porous Media

Bahador Najafiazar, Dept. of Petroleum Eng. & Applied Geophysics, Norwegian University of Science and Technology; Juan Yang, Christian Rone Simon, and Fuad Karimov, SINTEF Materials & Chemistry; Ole Torsæter, Dept. of Petroleum Eng. & Applied Geophysics, Norwegian University of Science and Technology; Torleif Holt, SINTEF Petroleum Research

This paper was prepared for presentation at the SPE Bergen One Day Seminar held in Bergen, Norway, 20 April 2016.

Abstract

Silica nanoparticles modified with a variety of chemical surface functionalities are interesting additives, which can bring enhanced properties such as increased sustainability, ductility and flexibility to polymer materials. These functional nanoparticles have already shown promising applications in paints, lacquers and coatings. By elaborating an appropriate surface functionalisation, silica nanoparticles can be adapted to the conditions in oil reservoirs, modify polymer transport, adjust their gelation behaviour and thus show a great potential for oil recovery processes.

The objectives of the present work are to investigate transport properties of functionalised silica nanoparticles and polymer in porous media by characterizing their stability, retention and other physical properties.

The transport properties of functionalised hybrid silica nanoparticles and polymer have been investigated through flooding experiments in two types of sandstones, high permeability Bentheimer and lower permeability Berea. The experiments were conducted at room temperature by use of 500 - 2000 ppm solutions of polymer and nanoparticles. Each experiment consisted of four stages; the active materials were injected at stages 1 and 3 whereas only brine was injected in stages 2 and 4. The polymer and the nanoparticles were quantified at the core outlet by inline viscosity measurements and by use of inline measurements of UV absorption or refractive index. The history of effluent concentrations was compared with un-retained flow by use of a conductivity contrast as tracer.

Mechanical entrapment, adsorption and inaccessible pore volume were estimated through analyses of component profiles and mass balance calculations. While polymer transport appears to be very different in the two cores expressed by quantities such as adsorption, mechanical entrapment and inaccessible pore volumes, nanoparticles appear to be transported through the entire pore space with low and partly reversible retention.

Introduction

Recently, there has been a lot of interest and excitement on how nanotechnology may be applied within the upstream oil industry (Ayatollahi and Zerafat, 2012; Cocuzza *et al.*, 2011; Fletcher and Davis, 2010). There is a clear understanding that nanotechnology is going to find a large range of applications, generally within petroleum technology and specifically in enhanced oil recovery (EOR). Extensive research on nanoparticles has offered different ways of controlling oil recovery processes. Such studies address, for instance, wettability alteration, mobility control and boosting efficiency of EOR chemicals or their transport into the formation (Feng *et al.*, 2013; Kapusta *et al.*, 2013; Kong and Ohadi, 2013). Transport properties of particles in porous media on a nanoscale level play an important role for these applications (Wu *et al.*, 2013).

Nanotechnology takes advantage of synthesizing materials on a molecular scale. With their very small size (less than 100 nm), nano-sized particles possess a very high surface specific area (compared to bulk) that gives them enhanced surface properties such as high reactivity. If properly controlled, such reactivity can be implemented in preparation of gel systems as networks of particles with the surrounding.

Deep placements of gels in hydrocarbon reservoirs can lead to blocking of water flow channels and diverting the water into other reservoir areas. This has the potential to reduce water production significantly and improve water flood in unswept areas. Placement of gels, however, is a challenging task since a high viscosity gel cannot be transported deep into the formation. There are several factors such as temperature, pH and salinity which strongly affect how fast a gel is formed. In many cases, the gelation time is too short to get an appropriate gel placement for the actual reservoir situation. One solution is to inject a low viscosity polymer together with both a crosslinking chemical and a crosslinking delay chemical so that the gelation takes place deeper into the formation (Jayakumar and Lane, 2013). Another solution is to encapsulate the cross-linker into polyelectrolyte complexes that acts as a carrier into the reservoir. In this manner the formation of strong gels may be delayed by several weeks (Johnson *et al*., 2010).

The overall goal of our ongoing research project is to develop a new type of nanoparticles which act as environmental friendly cross-linkers for partially hydrolysed polyacrylamide (HPAM) and possibly other polymers. The cross-linking functionality of the nanoparticles will be initially blocked and then released slowly under the reservoir conditions, ensuring a controlled gel placement. The development of such functionalised silica nanoparticles is based on a proprietary technology called FunzioNano™ (Männle *et al*., 2011) which has its centre in a cost effective synthesis of the organic/inorganic nanostructured hybrid polymers. By use of nanoparticles as crosslinking agents it may be possible to form stable gels without *e.g.,* chromium that may not be environmentally acceptable.

The objective of the present work is to investigate transport of polymers and functionalised nanoparticles in porous media by characterizing their stability, retention and other physical properties. Several nanoparticle and polymer flooding experiments were carried out with Bentheimer and Berea sandstones.

Functionalised Silica Nanoparticles

The functionalised silica nanoparticles with active groups were prepared by a typical sol-gel synthesis (Brinker and Scherer, 1990). A second step reaction involving surface functionalisation was performed with the obtained sol-gel nanoparticles in order to block the cross-linking functionality. The obtained nanoparticles were characterized by particle size analysis conducted via a Malvern instrument (Zetasizer) and nuclear magnetic resonance (NMR) for examining active and blocked cross-linking groups.

By carefully adjusting parameters such as concentration, temperature, solvent, *etc*., monodispersed nanoparticles with an average size of 2–5 nm and active cross linking functionality can be obtained (see Figure 1). After surface functionalisation, nanoparticles become slightly larger. Surface modification can be adjusted to block the active cross-linking groups fully or partially, which can be confirmed by NMR.

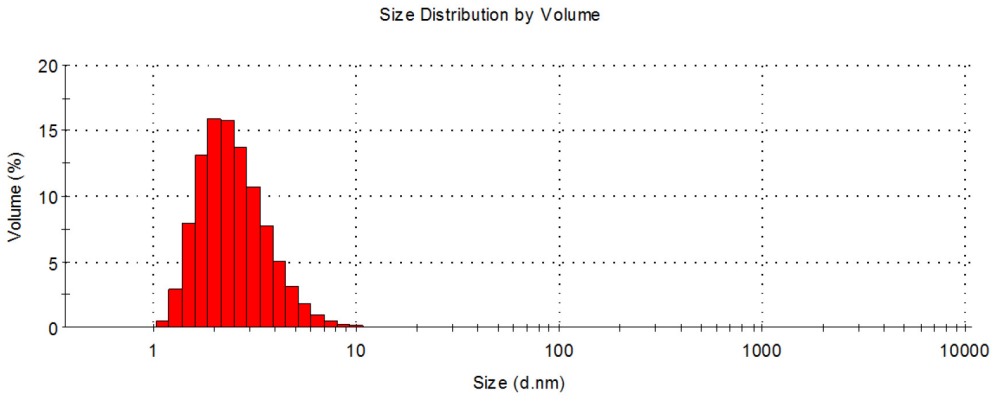

Figure 1—Particle size distribution of silica hybrid nanoparticles with active cross linking groups.

Figure 2 illustrates the concept of retarding gel formation. Figure 2(a), shows that a combination of nanoparticles with active cross-linking groups with HPAM will lead to the formation of gel. Figure 2(b) shows that when the active groups are blocked, no HPAM gels are expected. In Figure 2(c), the blocking groups undergo slow hydrolysis (or another decomposition reaction) and make the active cross linking groups available again. As a result, the formation of HPAM gel is retarded. For the purpose of this work, silica based hybrid nanoparticles with active cross-linking functionality (*e.g.,* amine groups) were synthesized. After that, the cross-linking functionality of the nanoparticles were fully blocked, since the objective of the present work is to study the transport mechanism of said nanoparticles through porous media in presence or absence of HPAM.

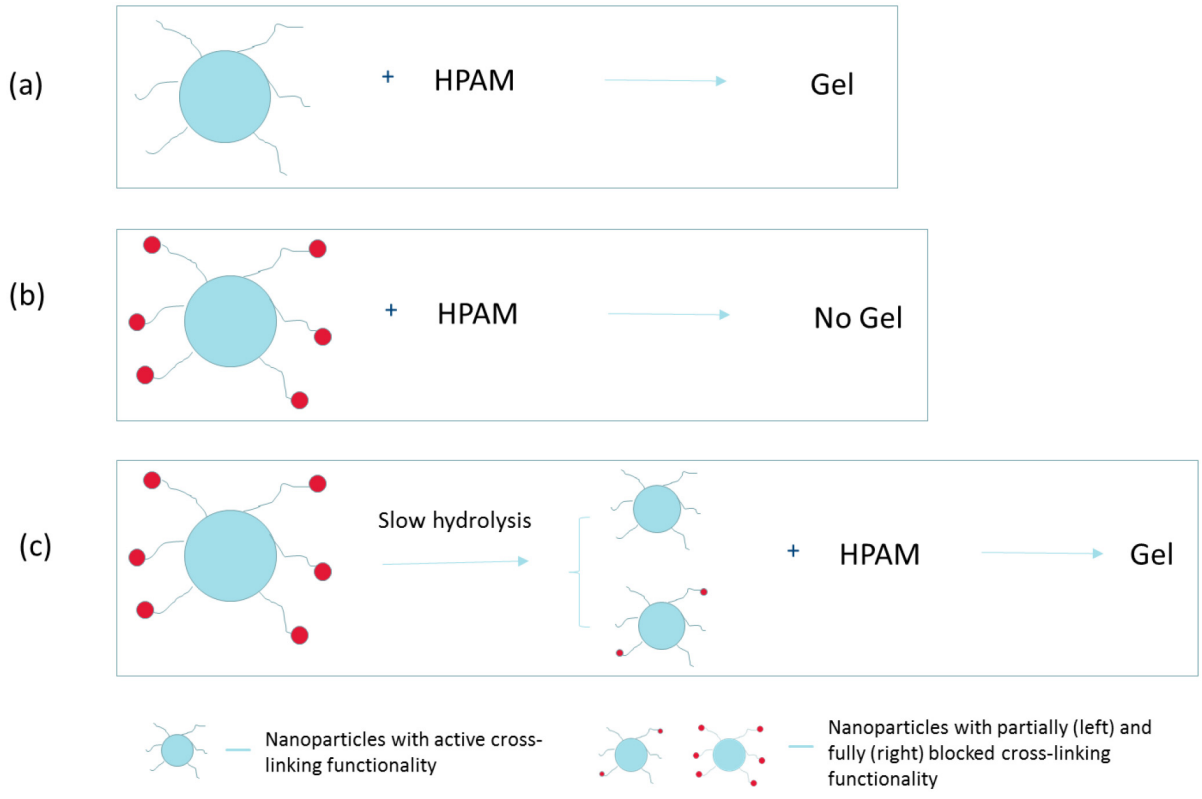

Figure 2—Schematic diagram of formation of retarded HPAM gel with nanoparticles.

Transport and Retention of Aqueous Dispersions of Nanoparticles and HPAM in Porous Media

The concepts of retention, adsorption, inaccessible pore volume (IPV), *etc.* in porous media and how they are determined by experiments for polymers is summarized by *e.g.,* Lotsch *et al.*, (1985). Figure 3 shows various idealized responses to changes in the composition of the injected solution (*e.g.,* polymer, nanoparticles, salt concentration). The grey profile illustrates the ideal response to a non-retaining, no excluded and non-dispersed step change at 0 Pore Volume (PV) injected. At 1 PV injected the concentration of produced fluid will step from 0 to 1 and remain at 1 as long as the composition of the injected fluid is not changed. The red profile shows the response to the change in a system where the only physical effect is dispersion (diffusion and mechanical dispersion). For a homogeneous system the red profile is symmetrical around the grey profile. The green profile is the idealized profile in a system with dispersion and where some of the pore space is excluded for the component under study (*e.g.,* the polymer). Owing to the reduced accessible pore volume, the green response occurs earlier than the ideal profile (grey) and the profile with only dispersion (red). The blue profile is the idealized response in a system with dispersion and where the component under study is retained due to adsorption and possible mechanical entrapment (filtering). As a result, the blue response occurs later than the other profiles. If some of the pores space is excluded for the component in question, the blue response will be shifted to the left.

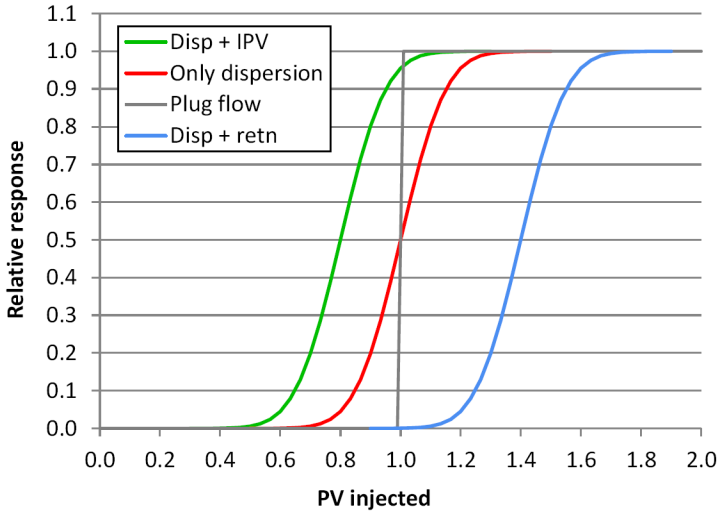

Figure 3—Responses to changes in injected concentration

For a step in the salt concentration, a profile equal to the ″only dispersion″ is expected. The polymer and NP profiles can have any combination of the profiles depending on the magnitude of the excluded pore volume and retention and the flooding history of the system.

Inaccessible pore volume of *e.g.* polymer can be determined by comparing the production profiles of polymer and a non-retained tracer after injection of polymer and tracer by plotting the relative responses ($c_i/c_{i,\ max}$) as functions of pore volumes injected. c_i is the measured effluent concentration of component i and $c_{i,\ max}$ is the injected concentration. A typical response profile of polymer and salt tracer after switching the injection to only brine with lower salt concentration is shown in Figure 4. The IPV can be determined from the difference in the areas below the response curves for polymer and tracer, provided that no adsorbed or entrapped polymer is released. Ideally, the tracer area, A_{tracer}, is exactly one PV. For polymer, the adsorption is essentially irreversible, and due to the inaccessible pore volume the polymer area, $A_{polymer}$, will be less than one as shown in the figure.

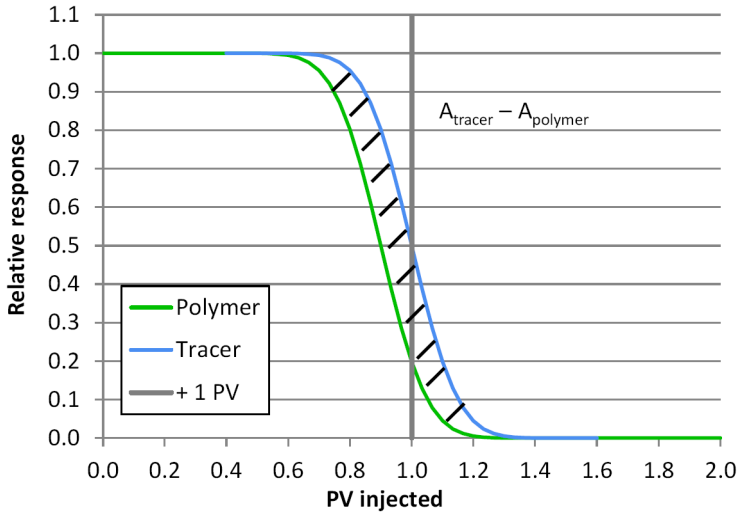

Figure 4—Typical responses after changing the injected solution from a polymer solution to a solution containing only a tracer ion at a different concentration. The difference in areas defines the inaccessible pore volume.

If the adsorbed or mechanically trapped component *i* is released during flooding with only brine, the area under the component curve may be larger than the tracer area. In that case the IPV becomes negative and loses its original physical meaning. However, a negative IPV indicates release of retained matter.

The magnitude of the retention will depend on the adsorption capacity of the rock and possible mechanical trapping in the porous medium. The magnitude of the retention in a multi-slug experiment, as here, will also depend on the stage under study. Thus, if the adsorption capacity for component *i* was saturated during the first slug, and the adsorption is irreversible, no more of component *i* would be adsorbed in the next injection stage. Mechanical entrapment may still persist, however.

Figure 5 shows the relative responses of changes in polymer concentrations in the transition periods after injection of the first and second polymer slugs. The area between the response curves will be a measure of how much more polymer was retained during the first slug injected. Provided that the magnitude of a possible mechanical retention was equal in the two stages, the area will be a measure of the amount of polymer adsorbed.

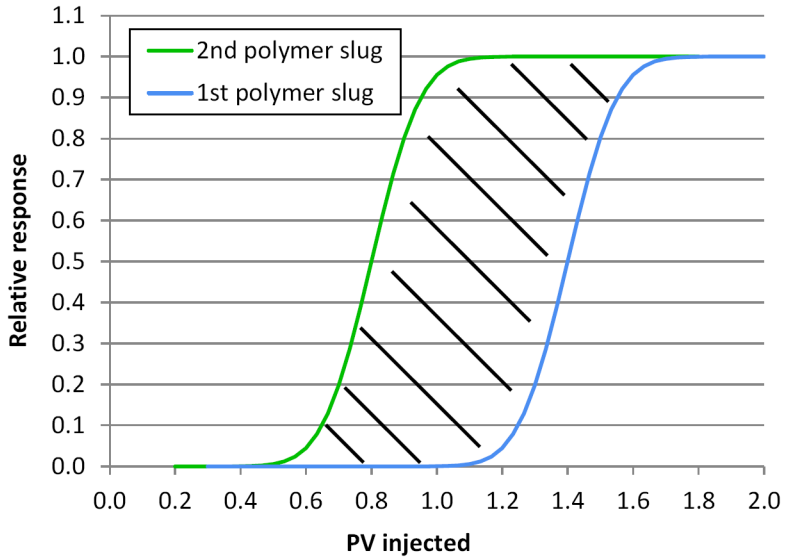

Figure 5—Typical difference in response of the first and second polymer slug.

Materials & Experimental Approach

Materials

Synthetic Sea Water (SSW) A sea water recipe (see Table 1) was used to create SSW, in order to have a fixed concentration of ingredients across all experiments.

Table 1—Synthetic Sea Water (SSW) recipe

Salt	Mass (g)
NaCl	23.612
$CaCl_2 \cdot 2H2O$	1.911
$MgCl_2 \cdot 6H2O$	9.149
KCl	0.746
Na_2SO_4	3.407

Nanoparticles FunzioNano nanoparticles were dissolved in SSW overnight with a magnetic stirrer and then 30 minutes ultra-sonication for improved dissolution. The solution was filtered through a 0.45 μm membrane filter before being used.

Porous Media Two types of sandstone were employed for our experiments: Berea and Bentheimer. Berea is considered to be a good model reservoir rock due to desirable porosity and permeability values. It is a sedimentary rock which is mainly composed of quartz, and also contains feldspar, carbonate and some clay minerals. Bentheimer is also an ideal rock for reservoir studies, since it is laterally continuous and homogeneously block-scaled (Peksa *et al.*, 2015). It is a marine formation from the Lower Cretaceous age. It has higher porosity and permeability as compared to Berea and contains mainly quartz and feldspar.

Polymer A powder of partially hydrolysed polyacrylamide (HPAM) with an assumed molecular weight in the order of 12 MDa was used as the polymer. Polymer solutions were prepared by dissolving the powder in SSW by first stirring the solution with a propeller at 500 rpm for two hours followed by magnetic stirring overnight. Before use the solutions were filtered by flooding through a 0.5 Darcy Berea core at 10 ml/min or maximum 20 bar pressure drop.

Characterization Techniques

Permeability of the core was calculated by measuring the core differential pressure vs SSW flowrate through the water saturated core and implementing Darcy's law. A minimum of 5 different flowrates were used. The flowrates were monitored by weighing the effluents.

Porosity of the core was measured by analysing the amount of Cl^- produced during $NaNO_3$ flooding from the initially 100 % SSW saturated core. The flow-lines (bypassing the core) were thoroughly flooded with 0.5 M $NaNO_3$ solution. Afterwards, the core was flooded with the same $NaNO_3$ solution and the effluent was collected. The injected volume was typically ten times as large as the expected pore volume. The amount of Cl^- in the produced fluid and SSW was determined by potentiometric titration (Metrohm 672 Titroprocessor) using 0.100 M $AgNO_3$. Knowledge of the Cl^- contents enabled calculation of produced volume brine, and hence pore volume (when core holder dead volumes were adequately corrected for).

Conductivity of the effluent was measured by determining the resistance of the fluid between two small rodded platinum electrodes integrated in a flow channel in a small housing made of polyoxymethylene (POM). The conductivity was measured by a Radiometer CDM 83 Conductivity Meter. The measurements were temperature corrected and referenced to a suitable average temperature as ionic mobilities and thus conductivity are significantly affected by temperature.

Viscosity of the effluent was found by measuring the pressure drop across a spiral 1/16″ OD (viscometer) tube. A calibration curve relating pressure drop to polymer concentration was made prior to each experiment. The spiral tube was immersed in a controlled temperature water bath in order to avoid temperature variations.

Refractive Index (RI) of the effluent was measured with a Shodex RI SE-51 refractive index detector with SSW as the reference medium. RI measurements were used to determine the concentration of nanoparticles in the effluent. A calibration curve was generated with various concentrations prior to the core flooding experiments.

UV light absorption of the effluent was measured with a multichannel UV-detector KNAUER Azura MWD 2.1L. UV light absorption at 195 nm was used to determine the concentration of nanoparticles and polymer in the effluent. A calibration curve was generated with various concentrations prior to the core flooding experiment.

Coreflood Experiments for Studying Transport Phenomena

Experimental Setup

Figure 6 illustrates a schematic of the experimental setup. Depending on the experiment, an SSW, polymer and/or nanoparticles reservoir constitutes the beginning of the setup. A nitrogen filled cushion was connected to the polymer reservoir. Each reservoir was connected to a Pharmacia P-500 pump. Each pump can run individually or simultaneously with other pumps in order to mix the input fluids in-line. The inlet flow line was connected to the bottom side of the vertically oriented core holder. The core holder enclosed the core, wrapped in Ni-foil, in a Viton rubber sleeve. A net overburden pressure of ~50 bar ensured that fluids flowed only through the core. The temperature control option of the core holder was not used for the current experiments, which were at room temperature. Downstream of the core, online measurement systems, *i.e.* a UV detector and/or refractive index detector, a conductivity cell and a viscometer, were included. Pressure readings were conducted at several locations along the system by use of pressure/differential pressure transducers. The effluents were collected and weighed at the outlet of the system. The experiments were done with 3 – 6 bar back pressure, lowest when the refractive index detector was used.

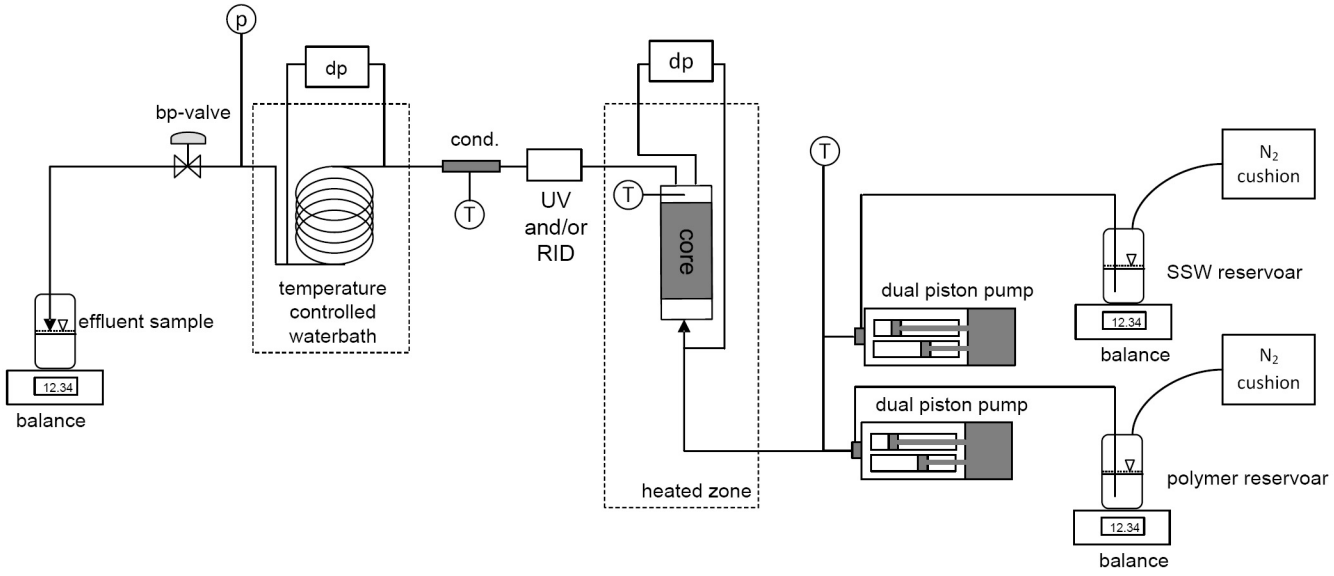

Figure 6—Schematic of coreflood set-up

Experimental Approach for Nanoparticle or Polymer flooding

First, a new core (of diameter 3.8 cm and length 20cm) was mounted in the core holder. After making sure that there were no leakages in the system, the core was first flooded with isopropanol until 100 % saturation. After that, several PVs of SSW were flooded through in order to ensure stable flow conditions. Next, porosity and permeability were measured. The experiments with only polymer started by saturating the core with 80% SSW, and then injecting polymer dissolved in 100% SSW. On the other hand, the experiments involving nanoparticles always used 100% SSW because the salt concentration also influenced the detector signals. The main part of the experiments started with injection of one slug of nanoparticles and/or polymer. The first slug (Stage 1) continued until the measurements became stable and several PV were injected. After that, the injected fluid was switched to pure brine (Stage 2) and the injection continued until stable measurements were achieved. Next, a second slug with additives (Stage 3) followed by a second slug with brine (Stage 4) ran until steady state measurements were achieved. The experiment ended after a final water permeability measurement. Process parameters and detector/sensor readings were continuously logged during the experiment.

Results and discussion

The results from five core flooding experiments are presented in Figure 7 through Figure 11. Each experiment started with injection of a slug with nanoparticles, polymer or nanoparticles + polymer (Stage 1). After some time this was followed by injection of only brine (with lower salt concentration in the experiments only involving polymer) (Stage 2), then a new slug with additives (Stage 3) and finally a slug without additives (Stage 4). The figures show normalized responses of nanoparticles (RI or UV detector) and/or polymer (viscometer), normalized conductivity responses and the differential pressure measured across the core. Event lines indicate the starting point of each stage and after one pore volume injected. Table 2 summarizes basic properties of the cores. The table also contains the final permeability of the cores at the end of the experiments, after injection of nanoparticles and/or polymer.

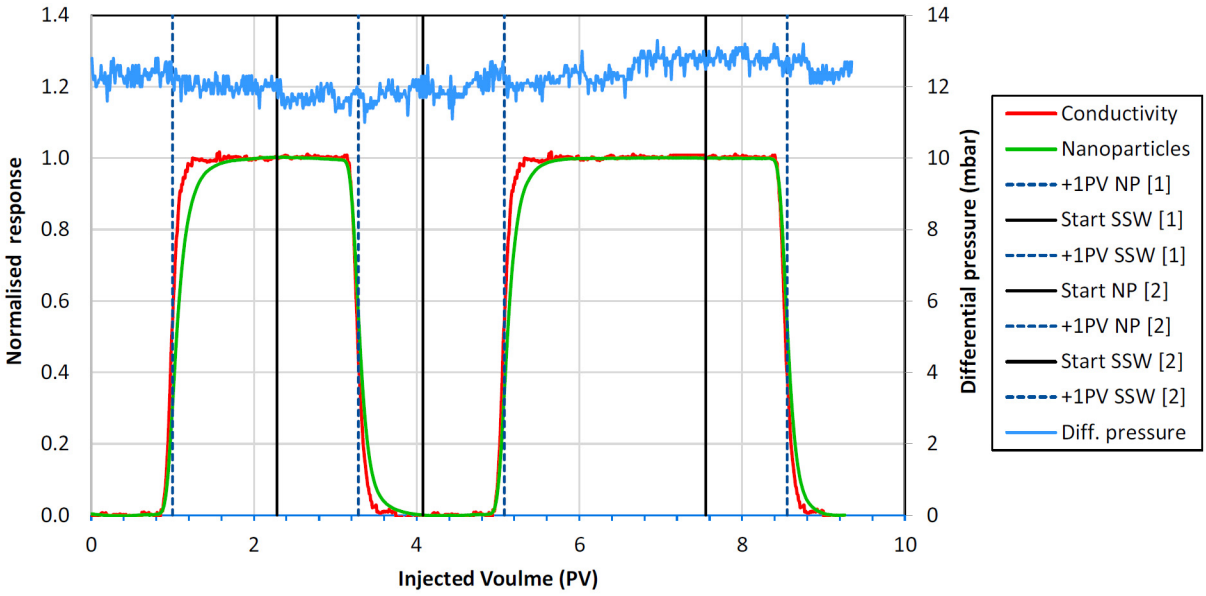

Figure 7—Experiment 1, injection of nanoparticles into Bentheimer sandstone.

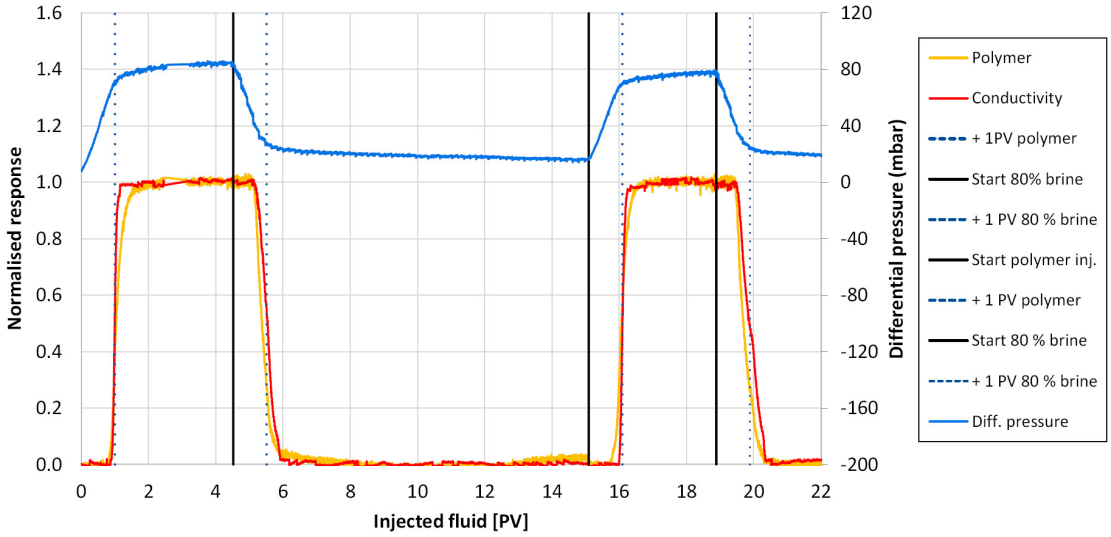

Figure 8—Experiment 2, injection of polymer into Bentheimer sandstone.

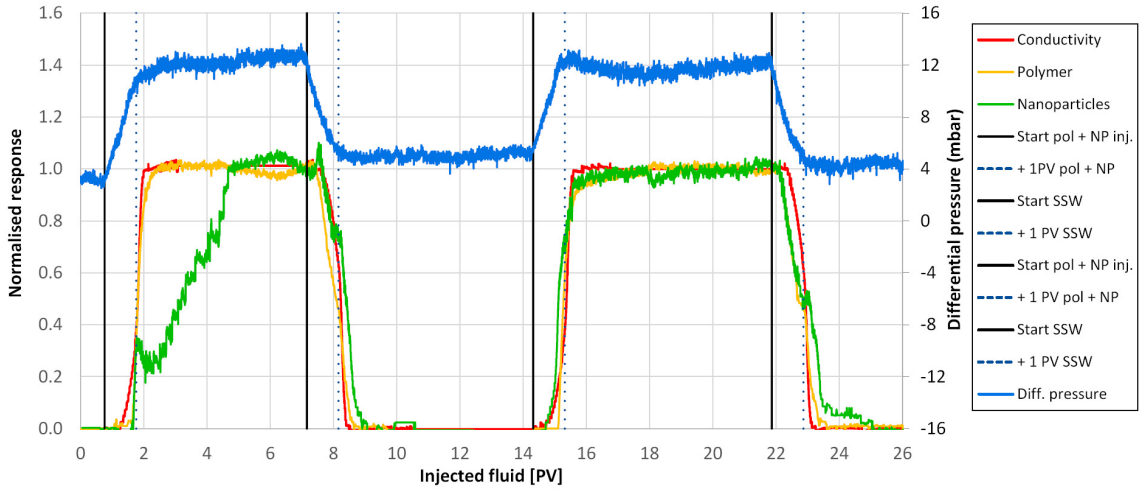

Figure 9—Experiment 3, injection of nanoparticles and polymer into Bentheimer sandstone.

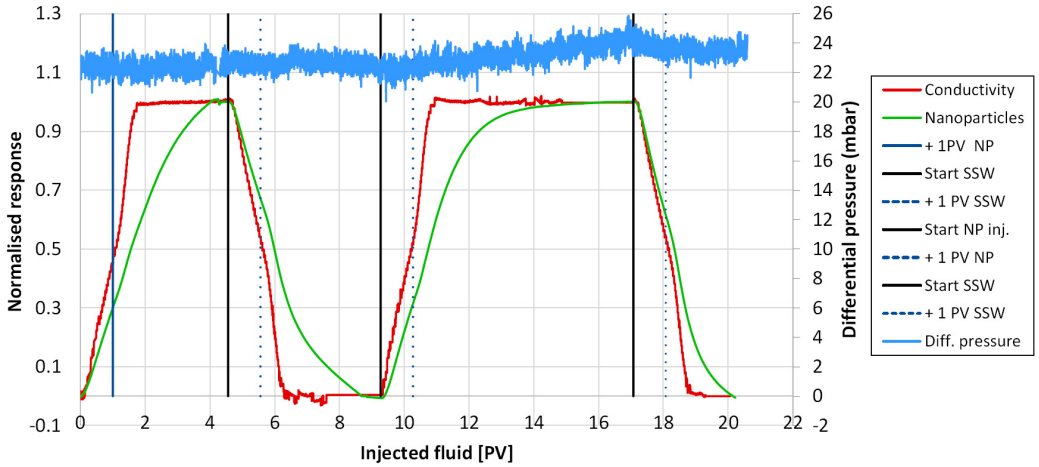

Figure 10—Experiment 4, injection of nanoparticles into Berea sandstone.

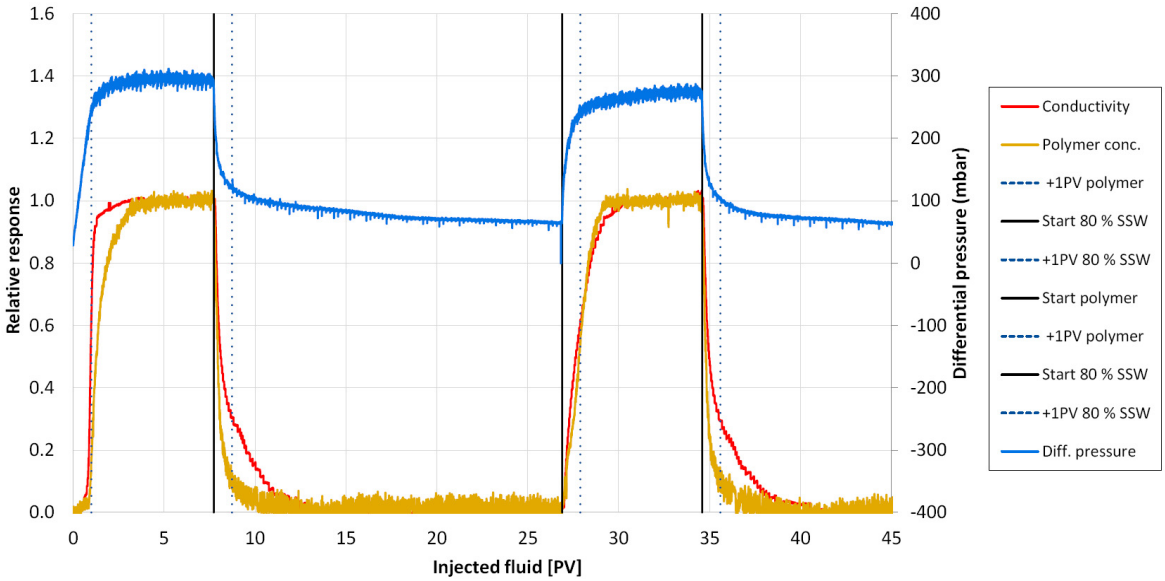

Figure 11—Experiment 5, injection of polymer into Berea sandstone.

Table 2—Basic rock properties.

Exp. no.	Rock	Injected additive	Pore vol. (ml)	Porosity (fraction)	Initial perm. (Darcy)	Final perm. (Darcy)
1	Bentheimer	nanoparticles	53.0	23.1	2.74	2.81
2	Bentheimer	polymer	53.0	23.1	2.81	0.51
3	Bentheimer	nanop.+ polymer	50.8	23.5	2.84	1.22
4	Berea	nanoparticles	43.9	19.7	0.36	0.33
5	Berea	polymer	42.4	18.6	0.29	0.09

For the experiments involving nanoparticles, the conductivity responses were determined in separate runs from the main core floods, since changes in salt concentration affects both UV absorption at 195 nm and the refractive index of the fluid. The conductivity responses were measured with the same injection rates with slugs of SSW and 80% SSW into the cores. However, for the two experiments with only polymer, the conductivity and polymer responses were determined in the same run.

In order to construct UV absorption and viscosity response models, solutions with different nanoparticle and polymer concentrations were flooded through the UV detector and the viscometer tube. For the UV absorption data, a model involving first and second order terms, with respect to both nanoparticles and polymer concentrations, as well as a cross term (product of the concentrations) yielded a good fit. For the pressure drop over the viscometer tube, the concentration of nanoparticles had no significant effect, which resulted in a second order model in only polymer concentrations. Since the polymer has a larger UV absorption compared to the nanoparticles, higher nanoparticle and lower polymer concentrations were used in Experiment 3 (see Table 3). The RI detector had a close to linear response with the concentration of nanoparticles.

Table 3—Polymer adsorption and inaccessible pore volumes determined for polymer and nanoparticles.

Exp. no.	Injected additive	Inj. conc. (ppm)	Pol. ads. (mg/g rock)	IPV polymer		IPV nanoparticles	
				Stage 2	Stage 4	Stage 2	Stage 4
1	nanoparticles	1000	-	-	-	-0.03	-0.02
2	polymer	1000	0.010	0.07	0.13	-	-
3	nanop.+ polymer	2000/500	0.005	0.10	0.09	-0.16	-0.08
4	nanoparticles	1000	-	-	-	-0.55	-0.26 (-0.08)
5	polymer	1000	0.042	0.54	0.59	-	-

Table 3 shows the magnitude of polymer adsorption determined as the difference in Stage 1 and Stage 3 responses of polymer (see Figure 5). The table also gives values of the inaccessible pore volumes (IPVs) determined from the responses at Stage 2 and Stage 4 (see Figure 4). The polymer adsorption determined for Berea is significantly larger than for Bentheimer sandstone. The presence of nanoparticles in the Bentheimer core did not result in increased adsorption of polymer. The IPVs for polymer in the Bentheimer cores were in the order of 0.1 PV and were not affected by the presence of nanoparticles. The IPV for polymer in the Berea core was larger than 0.5 PV.

For the nanoparticles, the IPVs were negative. This means that the amount of nanoparticles produced at the stages in question were more than the corresponding amount of nanoparticles in one pore volume. In other words, aside from one pore volume of nanoparticles that was in solution, some additional nanoparticles were produced. These extra nanoparticles were either adsorbed and/or entrapped at stages 1 and 3, which were desorbed and/or released at stages 2 and 4. The measurements cannot reveal whether some of the pore volume is inaccessible to nanoparticles, nor can they distinguish adsorption from the total retention.

Based on mass balances for each stage of the experiment, the amount of polymer or nanoparticles in the core after each stage (retained) was calculated. Table 4, Figure 12 and Figure 13 summarize the retention of matter at the various stages given as mg retained matter per g of rock. The retained mass of nanoparticles and/or polymer at the end of stage 1 was found by subtracting the produced mass (found by numerical integration of the response curve in question) from the injected mass (PVs injected times the injected concentration). The amount of nanoparticles and/or polymer in solution was found by the multiplying the accessible pore volume (=1 PV for nanoparticles, =[1- inaccessible PV] for polymer) by the injected concentration. For the later stages, the mass at the end of the preceding stage was included in the mass balance.

Table 4—Retention of nanoparticles and polymer (mg/g rock).

Exp. no	Additive	Stage 1	Stage 2	Stage 3	Stage 4
1	nanoparticles	0.009	0.005	0.007	0.005
2	polymer	0.021	0.018	0.029	0.032
3	nanoparticles	0.35	0.28	0.30	0.26
3	polymer	0.010	0.011	0.021	0.021
4	nanoparticles	0.07	0.01	0.08 (0.17)	0.05 (0.16)
5	polymer	0.09	0.09	0.14	0.14

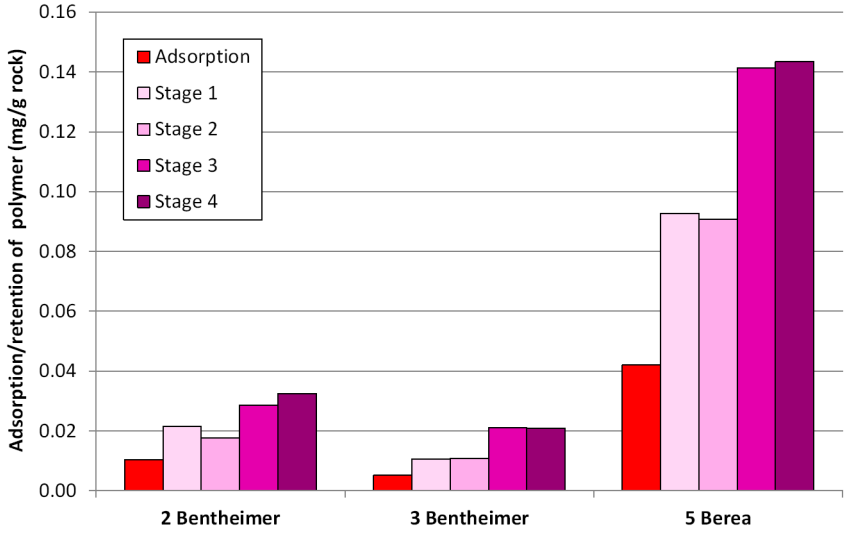

Figure 12—Adsorption and retention of polymer at the various experimental stages.

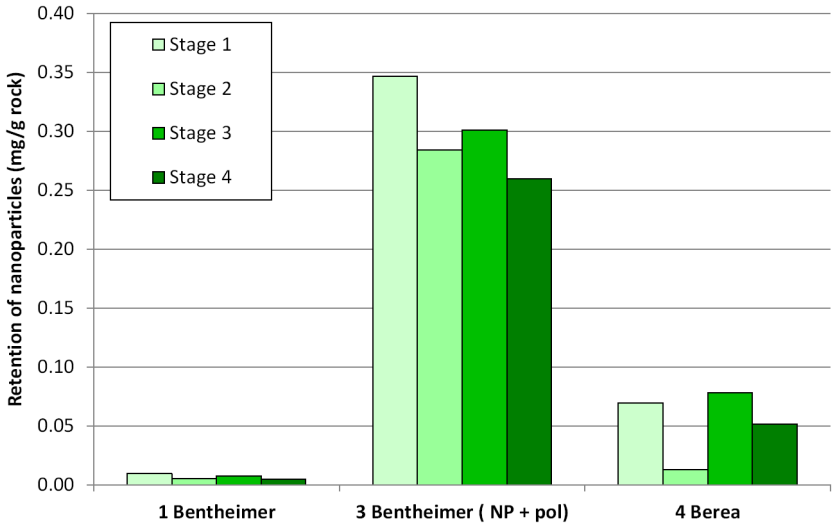

Figure 13—Retention of nanoparticles at the various experimental stages.

For polymer, both adsorption and mechanical entrapment were significantly higher in Berea compared to Bentheimer, as shown in Figure 12. In all the experiments, adsorption constituted approximately half of the total retention at the end of Stage 1. The total retention was practically unchanged at the end of Stage 2, indicating little or no desorption or release of mechanically trapped polymer. At Stage 3 the retention increased with values close to the difference between Stage 1 retention and adsorption. The polymer retained after Stage 3 remained in the core during the Stage 4 water injections. The presence of nanoparticles did not significantly affect the level of adsorption, retention or IPV in Bentheimer sandstone.

For injection of only nanoparticles into Bentheimer, the retention was low at all stages (Figure 13) but some release of retained nanoparticles appears to have occurred during the Stage 2 and Stage 4 water injections (see Table 4). In the presence of polymer, the Stage 1 retention was apparently high and remained high after Stage 2, although some nanoparticles were released during water injection. The increase in retention was low and close to zero during Stage 3 nanoparticle injection. The retention was further reduced during the Stage 4 water injection. The high Stage 1 retention can be a result of detector problems. This is discussed more below. For nanoparticle injection into Berea, the retention was higher

compared to the similar experiment with Bentheimer. Also in this experiment, detector problems biased the results. Retention is thus calculated for two interpretations of the detector responses. The figures for the interpretation regarded as less probable are given in parenthesis in Table 3 and Table 4.

The differential pressures across the cores were almost unchanged as long as only nanoparticles were injected. The absolute water permeabilities at the end of the experiments were thus close to the initial values (see Table 2). For the experiments involving polymer, the permeabilities measured at the end were significantly lower compared to the initial values. The ratio between the initial and the final absolute permeability is often called the residual resistance factor. For determination of the residual resistance factor the final permeability is often measured after a certain volume of injected water (*e.g.,* i100 PV) after the last polymer slug (Stage 3 in this work). No standardized throughput of water was used in the current experiments before measurement of the final permeability, however. By comparing the ratio of initial and final permeabilities it is seen that the ratio is higher for Experiment 2 involving only polymer compared to Experiment 3 with both nanoparticles and polymer. The permeability ration for the Berea core (Experiment 5) is also lower compared to the Bentheimer core (Experiment 2).

Figure 14 shows the measured UV-detector response during Experiment 3. After approximately four PV injected the detector peaked over the expected maximum value and remained high for another three PVs. Furthermore, between 15.5 PV and 21 PV, the detector signal fluctuated up and down in an unexpected manner. There are reasons to assume that the observed behaviour was resulting from problems with detector and not to physical phenomena in the experiment. Due to this the detector response was modified as shown in the figure. It can also be questioned if the detector signal was incorrect already after two PV injected and that this is the cause of the high Stage 1 retention. The calculated retention remained high for the subsequent stages due to the high Stage 1 value.

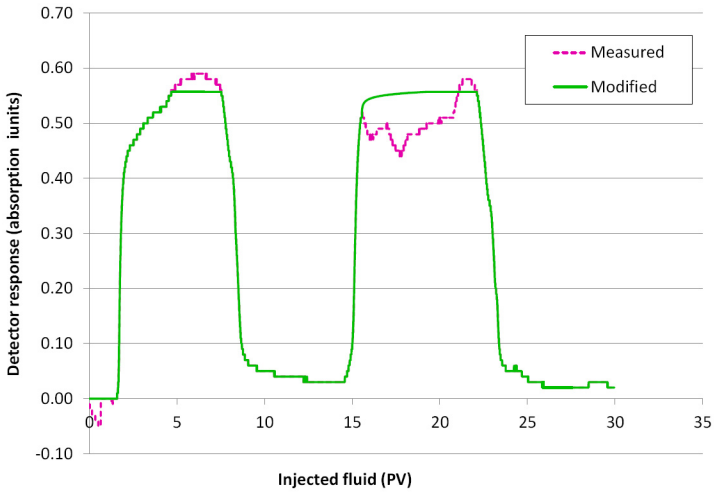

Figure 14—Measured and modified detector response during Experiment 3.

Figure 15 shows the refractive index response for Experiment 4. After approximately 4 PV the detector signal peaked sharply and thereafter it did not zero when only water was flowing. This was interpreted as the result of detector drift and the measured signal was modified as shown in the figure. During the second nanoparticle injection the detector signal levelled out at approximately 140 response units and not at 165 as expected from calibrations. However, in the mass balance calculations it has been assumed that the produced solution reached the increased concentration towards the end of Stage 3. In an alternative calculation it was assumed that the produced concentration only reached 85 % of the injected concentration at the end of Stage 3. The effect of this is on IPV and retention is given as figures in parenthesis in Table 3 and Table 4.

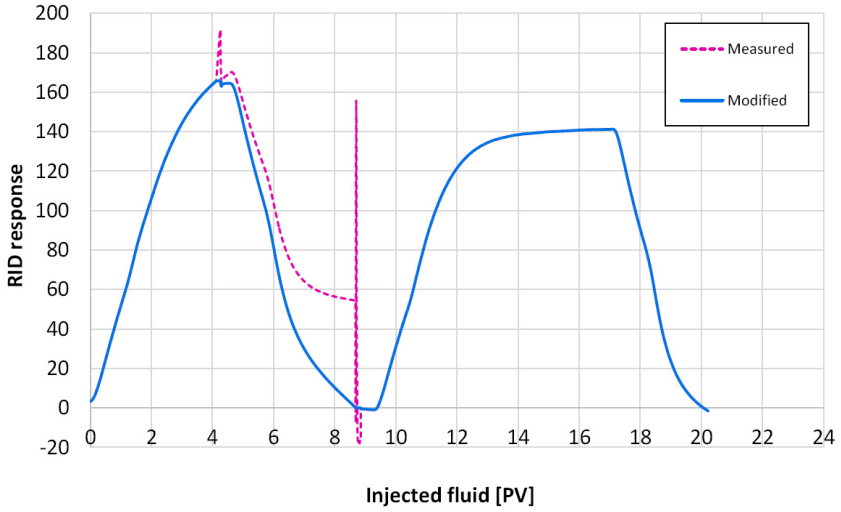

Figure 15—Measured and modified detector response during Experiment 5.

Online detection of nanoparticles either alone or together with polymer has proved to be the most challenging item in the present work. For polymer injected either alone or with nanoparticles continuous measurement of fluid viscosity by use of a capillary viscometer has proven to be feasible for determination of concentration.

The use of the refractive index detector gave very good and reproducible results for repeated nanoparticle injections into Bentheimer sandstone (several experiments were done). Sometimes baseline drift occurred but could be corrected for. Unfortunately, the duration of the various stages in Experiment 4 was somewhat short and more secure corrections of baseline drifts could possibly have been obtained with longer duration of the stages.

UV detection should in principle be a feasible technique since both the nanoparticles and the polymer exhibit well defined absorption at 195 nm. At this wavelength, salt strongly absorbs light, too, which makes the detection somewhat challenging. Nevertheless, good and reproducible absorption data were obtained during construction of the response model for nanoparticles and polymer. It would have been a more optimal system if the nanoparticles and polymer had absorption maxima at different wavelengths.

Conclusions

Transport of nanoparticles and polymer in Bentheimer and Berea sandstone has been studied through core flooding experiments with a methodology that is often employed to study polymer transport in porous media.

The results obtained to this point indicate that parameters like polymer adsorption, polymer retention and IPV are not significantly affected by the presence of nanoparticles. Adsorption and total retention as well as IPV is significantly higher for Berea as compared to Bentheimer. Polymer retained during injection appears not to be released during following water floods.

Nanoparticles are transported through Bentheimer sandstone with low retention. Nanoparticles adsorbed or otherwise retained during injection are partly released during following water floods. The retention of nanoparticles in Berea was significantly higher compared to Bentheimer. Also in Berea polymer retained during injection appears not to be released during following water floods. When only nanoparticles were injected the differential pressures across the cores did not change significantly compared to water injection.

When nanoparticles and polymer were injected into Bentheimer sandstone the retention of nanoparticles was apparently high during the first injection stage. For the following stages the mass of retained

nanoparticles remained high but decreased. The apparently high values of retention can be due to erroneous detector signals.

Simultaneous detection of polymer and nanoparticles is feasible by combining viscosity measurements with measurement of UV absorption and/or changes in refractive index of produced fluid.

Acknowledgements

The funding of this work was provided by the Research Council of Norway and the oil companies Eni Norge AS, GDF Suez E&P Norge AS, Det Norske Oljeselskap ASA and Lundin Norway AS. Their financial support and interest in the project work is gratefully acknowledged.

Nomenclature

A,	area
c_i,	measured effluent concentration of component i
EOR,	enhanced oil recovery
HPAM,	partially hydrolysed polyacrylamide
IPV,	inaccessible pore volume
MDa,	million Daltons (unified atomic mass unit)
nm,	nanometres
NMR,	nuclear magnetic resonance
PV,	pore volume
RI,	refractive index
RID,	refractive index detector
SSW,	synthetic sea water
UV,	ultraviolet

References

Ayatollahi, S., & Zerafat, M. (2012). Nanotechnology-Assisted EOR Techniques: New Solutions to Old Challenges. In SPE International Oilfield Nanotechnology Conference (pp. 1–15). Noordwijk, Netherlands. http://doi.org/10.2118/157094-ms

Brinker, C. J., & Scherer, G. W. (1990). *Sol-Gel Science: The Physics and Chemistry of Sol_Gel Processing*. Elsevier. http://doi.org/10.1016/B978_0_08_057103_4.50002_7

Cocuzza, M., Pirri, F., Rocca, V., Verga, F., & Torino, P. (2011). Is the Oil Industry Ready for Nanotechnologies?? In Offshore Mediterranean Conference and Exhibition (pp. 1–17). Ravenna, Italy.

Feng, Q., Chen, X., & Zhang, G. (2013). Experimental and Numerical Study of Gel Particles Movement and Deposition in Porous Media After Polymer Flooding. *Transport in Porous Media,* **97**(1), 67–85. http://doi.org/10.1007/s11242_012_0110_1

Fletcher, A., & Davis, J. (2010). How EOR Can be Transformed by Nanotechnology. In Proceedings of SPE Improved Oil Recovery Symposium (pp. 24–28). Tulsa, Oklahoma, USA. http://doi.org/10.2118/129531-MS

Jayakumar, S., & Lane, R. H. (2013). Delayed Crosslink Polymer Flowing Gel System for Water Shutoff in Conventional and Unconventional Oil and Gas Reservoirs. In SPE International Symposium and Exhibition on Formation Damage Control. Lafayette, Louisiana, USA: Society of Petroleum Engineers. http://doi.org/10.2118/151699-MS

Kapusta, S., Balzano, L., & Te Riele, P. M. (2013). Nanotechnology Applications in Oil and Gas Exploration and Production. In International Petroleum Technology Conference. Bangkok, Thailand: International Petroleum Technology Conference. http://doi.org/10.2523/15152-MS

Kong, X., & Ohadi, M. (2013). Applications of Micro and Nano Technologies in the Oil and Gas Industry - Overview of the Recent Progress. In Abu Dhabi International Petroleum Exhibition and Conference. Abu Dhabi, UAE: Society of Petroleum Engineers. http://doi.org/10.2118/138241-MS

Lotsch, T., Muller, T., & Pusch, G. (1985). The Effect of Inaccessible Pore Volume on Polymer Coreflood Experiments. In *Proceedings of SPE Oilfield and Geothermal Chemistry Symposium*. Society of Petroleum Engineers. http://doi.org/10.2118/13590-MS

Männle, F., Simon, C., Beylich, J., & Redford, K. (2011, April 13). *Polybranched, organic / inorganic hybrid polymer and method for its manufacture*. Retrieved from http://www.google.com/patents/EP1740643B1?cl=en

Peksa, A. E., Wolf, K.-H. A. A., & Zitha, P. L. J. (2015). Bentheimer sandstone revisited for experimental purposes. *Marine and Petroleum Geology,* **67,** 701–719. http://doi.org/10.1016/j.marpetgeo.2015.06.001

Wu, J., He, J., Torsater, O., & Zhang, Z. (2013). Effect of Nanoparticles on Oil-Water Flow in a Confined Nanochannel: a Molecular Dynamics Study. In SPE International Oilfield Nanotechnology Conference and Exhibition. Society of Petroleum Engineers. http://doi.org/10.2118/156995-MS